VYSOKÉ UČENÍ TECHNICKÉ V BRNĚ
BRNO UNIVERSITY OF TECHNOLOGY

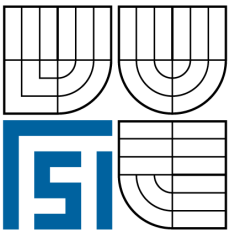

FAKULTA STROJNÍHO INŽENÝRSTVÍ
ÚSTAV FYZIKÁLNÍHO INŽENÝRSTVÍ
FACULTY OF MECHANICAL ENGINEERING
INSTITUTE OF PHYSICAL ENGINEERING

APLIKACE PLAZMONOVÝCH POLARITONŮ V NANOFOTONICE

APPLICATION OF PLASMON POLARITONS IN NANOPHOTONICS

TEZE DIZERTAČNÍ PRÁCE
DOCTORAL THESIS

AUTOR PRÁCE
AUTHOR
ING. LUKÁŠ BŘÍNEK

VEDOUCÍ PRÁCE
SUPERVISOR
Prof. RNDr. PETR DUB, CSc.

BRNO 2015

Klíčová slova
Plazmonické rezonanční antény, plazmonika, lokalizované plazmonové polaritony, SEIRS, FDTD simulace.

Keywords
Plasmonic resonant antennas, plasmonics, localized plasmon polaritons, SEIRS, FDTD simulations.

BŘíNEK, L.:*Aplikace plazmonových polaritonů v nanofotonice.* Brno: Vysoké učení technické v Brně, Fakulta strojnÍho inženýrstvÍ, 2015. 30 s. Teze dizertační práce. Vedoucí práce Prof. RNDr. Petr Dub, CSc.

Contents

1 Introduction

Nowadays, we are witnessing a rapid development of the information technology that puts ever-increasing demands on the information transfer and its processing. The signal processing is commonly carried out by technologies related to the electron transport that slowly reach their physical limits. Therefore, new technologies allowing faster signal processing are in focus of the scientific community.

Contrary to electrons, photons having no charge disregard electric and magnetic fields; moreover, their matter-interactions have been extensively studied and are well-known. For this reason, technologies exploiting photons may represent a useful supplement to the modern communication technology. One of perspective branches of optics is plasmonics that deals with the interaction between the electromagnetic field and electrons in metals at a metal-dielectric interface. The solution of the electromagnetic field at the conductive surface in the form of surface-waves was firstly found by Zenneck [1] and Sommerfeld [2].

The solutions of the Maxwell equations at the metal-dielectric interface are of the form of electromagnetic surface waves coupled to longitudinal collective oscillations of free-electron gas in a metal at metal-dielectric interfaces [3], [4], [5], [6], [7]. These surface waves propagate in the direction of the interface while the field exponentially decreases in the direction normal to the surface. The corresponding quasiparticles are called surface plasmon polaritons (SPPs) [5].

The existence of surface plasmon polaritons was firstly observed in a diffraction experiment on a metallic grating by R. W. Wood [8]. Later, a decrease in energy of electrons passing through thin metal foils in transmission electron microscopy was observed in 1950s [9], [10]. As the dispersion relation of SPPs exists below the light line in the given medium, the electromagnetic field is tied to the space smaller than the Rayleigh diffraction condition states [1]. For the same reason, SPPs cannot be excited or observed via the conventional way in the far-field unless the interface possesses some inhomogeneities. Consequently, experiments with the optical excitation of SPPs were performed by E. Kretschmann [11] and A. Otto [12] whose principles are commonly used till now. Even though the first studies of surface plasmon polaritons had been done at the beginning of the 20th century, fabrication of real plasmonic structures [13] started about 20 years ago when research in the field of nanotechnology expanded [14], [15].

The two-dimensional nature of SPPs promises the engineering of plasmonic optical-circuits still partially missing in optical communication systems, nano/photonic and optoelectronic devices in high-speed low-power telecommunications industry [13], [16], [17], [18], [19], [20]. Moreover, the response of plasmonic structures exhibits a high sensitivity to presence of materials in their vicinity. This behaviour may be exploited in sensing methods [21], [22], [23].

Surface plasmon polaritons may not only propagate along the surface but also they can be tied to metallic objects of subwavelength dimensions which implies the crucial enhancement of the electromagnetic field. Such a structure represents an insulator/metal/insulator truncated waveguide [3], [6] that converts free-propagating optical radiation to a localized energy and vice versa [24]. These structures are usually called resonant plasmonic antennas/structures. Plasmon polaritons resonating at these metallic structures are called Localized Plasmon Polaritons (LPPs).

[1] Thus, plasmonics enables the optics beyond the diffraction limit and a light-concentration in the space considerably tinier than the Rayleigh criterion.

Numbers of reviews have been published on plasmonic antennas in last four years [24], [25], [26], [27], [28]. Plasmonic antennas are utilized both for their scattering and absorption properties in the far-field or for high intensities in the near-field [18] at the resonance. Consequently, these structures are essential for many sensing applications [29] such as a high-resolution single-molecular microscopy and spectroscopy [30], surface-enhanced Raman spectroscopy [31], tip-enhanced Raman spectroscopy [32] and biosensing [22]. Moreover, a strong enhancement of the electromagnetic field via plasmonic resonances may be used in the photovoltaics [33], [34], [35], the enhanced photoluminescence [36], [37] and for trapping [38], [39], [40]. Last but not least, there are absorption-related applications [33] where a temperature enhancement occurs both in antennas and their surroundings [41], [42], [43]. This topic is studied also in this work (see Section 4). Temperature increase at resonance found a possible application also in a cancer-treatment in the medicine [23], [44]. To summarize, a majority of plasmonics applications is related to resonant structures.

Plasmonic antennas represent the main topic of the presented work. This work involves both theoretical and experimental study of these structures. The electromagnetic field of antennas and its near- and far-field properties have been modelled via numerical simulations. These simulations were then exploited to propose a geometry of antennas having given resonant properties. Afterwards, antennas (of geometry) proposed by simulations were fabricated by the electron beam lithography or focused ion beam. Subsequently, the optical properties of fabricated antennas have been measured and compared with the simulated ones.

Regarding the current trend, that the development of plasmonics is focused on sensing applications, the resonance properties of antennas in the vicinity of a material possessing vibrational modes and thus having the pronounced dispersion of its refractive index have been studied in this work. First, a numerical study of absorption properties of this antenna-substrate system is done in Section 4. Subsequently, measured reflection spectra of IR antennas fabricated by the Electron beam Lithography on not-annealed and annealed silicon-rich oxinitride (SRON) substrate are compared in Sections 4 and 5, respectively. These antennas may enhance the vibrational modes from the substrate (Sections 5.1 and 5.3).

2 Plasmonic resonant structures

Plasmonic resonant structures (plasmonic antennas, metallic spheres, etc.) are used in the majority of plasmonics applications [24], [25], [26], [27], [28]. Thus, plasmonic antennas and their properties represent the main tasks of this work where the emphasis is put on an enhancement of the electromagnetic field in the near-field (Section 4) and on sensing applications (Sections 4 and 5).

Plasmonic antennas have received a significant attention for their ability to concentrate the light energy into deep-subwavelength dimensions and for their resonance-sensitivity to environments they are embedded in [45]. In consequence, the plasmonic resonance may enhance the absorption of the electromagnetic field energy that can be used in the photoluminescence [36], the excitation of electron-hole pairs in semiconductors [19], in photovoltaics [33] and others [46].

Considering the absorption, much work has been done on plasmonic resonant struc-

tures (antennas) with respect to their heating properties. Most of such articles deal with the electromagnetic field absorption (and the corresponding heat development) in metallic parts of resonant structures embedded in transparent, non-absorbing environments [41], [42], [47], [48]. The enhancement of the heat generation via plasmonic resonances and a consequent temperature increase have not been studied only by simulations [41], [42], but also experimentally [43], [49]. The heat power enhanced by this method was utilized for instance in infrared spectrometers, bolometers [50], [51], [52], local growth of nanowires, in the phase transformation of materials in the antenna vicinity [48], [53], [54] and in other applications.

Furthermore, plasmonic structures found useful application in the enhancement of the signal in the Raman spectroscopy. There are two techniques: the Surface-Enhanced Raman Scattering (SERS) and the Tip-Enhanced Raman Spectroscopy (TERS). In SERS, the plasmonic effect occurs on a rough metallic surface. It enables the enhancement of the Raman signal by 4-8 orders of its magnitude [55], [56], [57], [58], [59]. Consequently, even a single-molecule sensitivity has been observed [60]. The second technique called the Tip-Enhanced Raman Spectroscopy (TERS) enables mapping of plasmonically enhanced Raman signal by using a scanning-probe technique. The field is enhanced by the plasmonic resonance of either metallic structures placed at an AFM probe or a metal-coated AFM probe itself [32], [61], [62]. Then, the Raman spectra should be mapped with a resolution below the diffraction limit.

Besides methods for the enhancement of the Raman signal, plasmonic infrared spectroscopic techniques like the Surface Enhanced Infrared Absorption (SEIRA) [63] and the Surface Enhanced Infrared Spectroscopy (SEIRS) are frequently studied nowadays [65], [66], [67], [68]. These techniques may provide information about chemical compositions (vibrational spectroscopy) of specimens. Furthermore, scanning-probe modifications of these plasmonic infrared spectroscopies allow to map the specimens. It has been demonstrated that scattering-type scanning near-field optical microscope is able to map the vibrational spectra with a spatial resolution roughly 1000 times better than conventional methods such as the FTIR [30]. For instance, objects as viruses as small as 18 nm have been observed in [69].

Obviously, the applications presented above require a comprehensive study of plasmonic antennas with purpose to reveal their resonances, electromagnetic field enhancement and distribution, mutual interactions, interactions with surrounding materials, etc. This represents the motivation for a basic research of antenna resonances [25], [28], [70], [71], [72], [73]. For instance, the sharp features (peaks/dips) in spectral responses of plasmonic structure interacting with the environment are compared with the hybridization states in the molecular orbital theory (including Fano resonances) in [72], [74], [75], [76].

3 Resonances of antennas

When dealing with resonant structures the first issue is often the investigation of resonance wavelengths of plasmonic antennas. In case of antennas deposited on transparent substrates the approximative prediction is simple. In particular, the resonance wavelength λ_{res} is proportional to the antenna arm length L (dimension in the direction of polariza-

tion of the incident field) and to the effective refractive index of the of SPPs n_{eff} by the approximative relation [7], [31], [77]

$$\lambda_{\text{res}} = 2n_{\text{eff}}L \tag{1}$$

where $n_{\text{eff}} = \sqrt{\frac{\varepsilon_{\text{sub}}\,\varepsilon_{\text{m}}}{\varepsilon_{\text{sub}}+\varepsilon_{\text{m}}}}$ with ε_{sub} and ε_{m} being dielectric functions of a substrate and a metal, respectively. In particular, $\texttt{Re}\,[\varepsilon_{\text{m}}] \ll -1$ holds for the dielectric function of a metal in infrared, whereas the dielectric function of the transparent substrate is constant. Consequently, the resonance wavelength is proportional to the refractive index of a substrate [77].

It has been demonstrated that interesting phenomena occur if the antennas interact through their near fields with dielectrics possessing absorption peaks or bands at specific wavelengths. When the substrate an antenna is deposited on is non-transparent, a non-linear dependence between resonance wavelengths and antenna arm lengths occurs. Such a situation is studied in following Section 4 where the antennas are deposited on a thin absorbing layer (on transparent silicon substrate) possessing the dispersion of its refractive index in MID-IR (particularly $\lambda \approx 8-12\ \mu$m). This Section is based on [78] that belongs to the first articles dealing with this behaviour [64], [65]. This work was motivated by an effort to exploit electromagnetic energy enhancement via platinum plasmonic antenna resonances for the phase transformation of the silicon-rich oxinitride into the nanocrystalline silicon. Afterwards, this work was extended on the sensing application in Sections 5 and 5.3.

The interaction of the resonant antenna with the absorbing material is known from a series of works dealing with intuitive models based on coupled molecular and plasmonic resonators predicting new effects such as a transition between Electromagnetically Induced Transparency (EIT) and enhanced absorption [79], or with Surface Enhanced Infrared Absorption (SEIRA) [80], Surface Enhanced Infrared Spectroscopy (SEIRS) [81], Fano-type signals in the IR extinction spectrum [65], [66], etc.

4 IR antennas on an absorbing substrate

This Section is aimed at plasmonic antennas deposited on an absorbing substrate with emphasis on resonance properties (in the far-field) and on electromagnetic field enhancement and consequent absorption increase in the near field [2].

If the metallic antennas are in a vicinity of dielectric materials having a pronounced dispersion of their dielectric function or the antennas are fabricated on substrates made out of them, the electromagnetic energy is absorbed. Consequently, the heat produces not only in metallic antennas, but also in these materials [83], [84]. As the highest electric field enhancement generally occurs in the gaps of antennas, the maximal absorption (heat generation) in the dielectrics caused by this field is spatially localized to small volumes of these absorbing materials underneath the gaps.

On the other hand, in this case the plasmonic antenna resonances themselves become significantly influenced by their coupling to absorption resonance processes in the material. The knowledge learned from the behaviour of plasmon resonance peaks in the

[2] This Section is based on author's publications [78], [82].

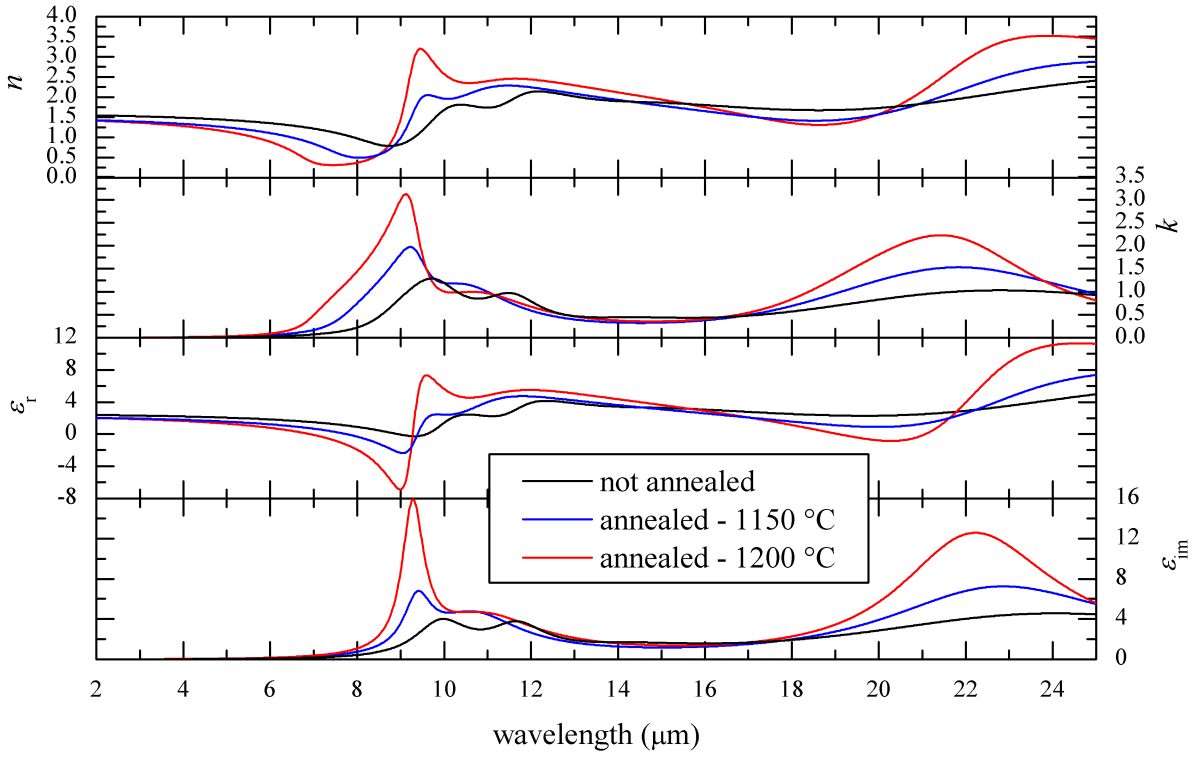

Figure 1: Refractive index and dielectric function of SRON layers not-annealed and annealed at temperatures 1150 °C and 1200 °C depicted by black, blue and red curves, respectively.

vicinity of the absorption peaks is then utilized in optimization of a spatially localized absorption of IR radiation/heat generation in such a substrate.

In the presented work, the silicon-rich oxinitride (SRON) with the significant absorption in the mid-infrared (see Fig. (1)) is used as the non-transparent 110 nm thin film deposited on Si substrate (resistivity 6–9 Ωcm). The SRON film was prepared by PECVD technique at the deposition temperature of 350° C, pressure = 650 mTorr, rf power 40 W at the frequency = 13.5 MHz and the (N_2O : SiH_4) flow ratio equals to 6.7 N_2O : SiH_4.

Its refractive index was experimentally obtained by fitting the reflection by 4 Lorentz oscillators (described by parameters in Table 1) and $\varepsilon_\infty = 2.44$ [78]. The first oscillator (at 1009 cm^{-1}) is related to Si-O stretching mode. The second oscillator (at 857 cm^{-1}) is related to Si-N stretching mode [85], [86] [3]. The third oscillator (at 698 cm^{-1}) was assigned to neutral oxygen vacancies (described as ≡Si-Si≡) [87]. The fourth oscillator (at 427 cm^{-1}) is related to Si-O rocking mode.

Golden plasmonic antennas (height: 60 nm of Au on a 3nm Ti buffer layer, width: 400 nm, length: 0.8 – 6 μm) were fabricated via electron beam lithography (FIB/SEM Lyra3 XMH Tescan) on the SRON layer. The antennas consist of two rectangular arms (dimmer antennas) separated by a gap of 100 nm to achieve the pronounced electromagnetic field there while fabrication of a smaller gap was difficult for longer antennas. The

[3]The Si-N stretching mode may vary within range of 835-890 cm^{-1}, on the other hand, it reaches the frequency of 835 cm^{-1} known for bulk Si_3N_4 films.

Table 1: Parameters of oscillators in the Lorentz model where a wavenumber reads $\nu = 1/\lambda$ [78].

$G_m\Omega_m^2$ [10^5cm^{-2}]	ω_{0m} [cm^{-1}]	λ_{0m} (μm)	γ_m [cm^{-1}]
5.35	1009	9.9	152
2.68	857	11.7	116
0.91	698	14.3	191
3.84	427	23.4	207

antenna geometry is depicted in Fig. 2. The rectangular shape of the antenna arms was chosen to enhance energy absorption inside a larger volume beneath the gap in SRON compared to bow-tie antennas, although its radiation efficiency is smaller [47]. The antennas of the same dimensions and shape were arranged into an array of the area of 50×50 μm^2 in order to increase the reflection signal-to-noise ratio. To find a configuration with a minimized coupling between the individual resonant antennas, a series of arrays with different spacing between the antennas were designed and tested for the same antenna geometry.

Unpolarized reflection spectra were obtained by a Fourier Transform IR microscope (FT-IR Bruker Vertex 80v + Hyperion 3000) working in the spectral range of 2 – 16.5 μm. The spectra taken from the antenna arrays were normalized to the reference ones related to the bare SRON surface nearby the antenna structures. The spectra for antennas of various arm lengths (with the same filling by metal in every array) are plotted in Fig. 3. Almost each spectrum in this figure possesses two resonant peaks separated by a deep valley caused by a strong coupling of plasmonic oscillations with absorption resonances in the SRON material in the corresponding wavelength range (see Fig. 1), leading to overdamping of these oscillations [79]. The presence of two resonance peaks for the antenna of a specific arm length is a direct consequence of a non-monotonic character of the real part of refractive index in the range of significant absorption (resulting from the Kramers-Kronig relations) and the related increase of its values for longer wavelengths. This is obvious from an approximation Equation 1 [77], where n_{SRON} is the real part of the SRON index of refraction. Because of the pronounced dispersion of the SRON dielectric function around the region of enhanced absorption (Fig. 1) a non-linear scaling between the resonance wavelength λ_{res} and the antenna arm length L should be expected [78], [82]. Indeed, looking at Fig. 4, where the peak positions are plotted, one can see that once the left resonance peak approaches the wavelength at which the absorption in SRON becomes substantial, it almost stops moving with increasing the antenna arm length and does not exceed the value $\lambda = 8.6$ μm. This is in agreement with the dependence depicted by the lower branch of the solid red curve in Fig. 4 obtained from the mentioned approximation formula. In addition, the intensity of the peak goes down and practically vanishes for the longest antenna lengths.

Accordingly, the right resonance peak is almost not moving with the small antenna arm lengths as the corresponding resonance wavelengths (12.5 μm) are too close to the area of enhanced absorption in SRON. However, this peak starts to move when the arms become bigger ($L \geq 2\mu$m) and thus the resonance wavelengths shift beyond this area.

As a consequence of the behaviour of these two peaks, two separated localized-surface-plasmon-resonance branches appear in the plot in Fig. 4. Similar effect has also been al-

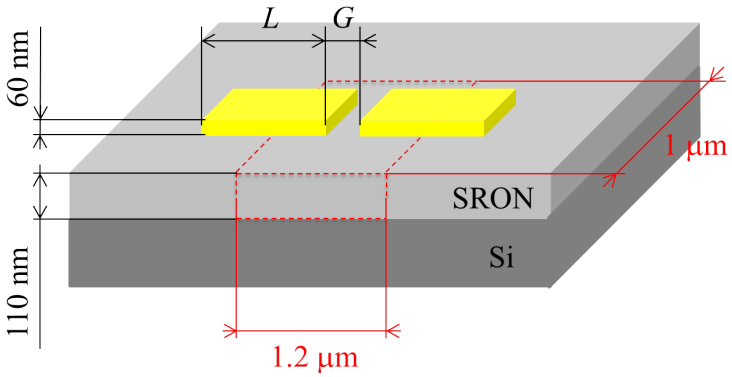

Figure 2: Au dimmer antenna placed on the SRON layer (110 nm thick) deposited on the Si substrate. The antenna height is 60 nm, its width is 400 nm and its length L varies from 1 μm to 6 μm. The distance between antenna arms (gap size G) is about 100 nm. The absorption enhancement is expected in the space below the antenna gap. Dimensions of the integration domain (depicted by red lines) are 1.2 μm along the main axis of antenna, 1 μm in the direction of the antenna width, and its height is 110 nm.

ready observed in dispersion relation curves (reciprocal space) of SPP on a sub-wavelength hole array covered with organic molecules having an absorption peak in the visible range [88].

One can notice from Fig. 3 that the spectra possess a shallow drop in their intensity around $\lambda \approx 11.5$ μm which is caused by a minor increase of the absorption in SRON around this wavelength. The resonances observed for the longer wavelengths shift qualitatively with the upper branch of the red curve in Fig. 4 obtained from the approximation formula 1, where $n_{\text{eff}} = n_{\text{SRON}}$ [78], [82].

The reflection spectra of the antennas were simulated by the FDTD method (Lumerical) [89] as well and the corresponding peak positions are plotted by blue line in Fig. 4. The good agreement between the experiment and the simulation up to $L = 4.5$ μm is obvious. For the antennas with $L > 4.5$ μm the experimental data are already weak as the quality of the peaks was very poor at the corresponding resonance wavelengths close to the upper end of the spectrometer measuring range. Contrary to the red analytical curve the numerical values of the resonance wavelength do not keep growing so intensively at the biggest arm lengths which is most likely caused by an increasing absorption in SRON at these wavelengths (see Fig. 1). In the inset of Fig. 3, the qualitatively same simulated and measured reflection spectra are shown for the antenna of $L = 3.2$ μm.

To get the information about the heat volumetric density generated by the spatially localized absorption in SRON beneath the antenna gap (upon antenna resonances), the electric field in this volume was simulated. The heat density is determined by the formula

$$q(\mathbf{r}) = \frac{1}{2}\varepsilon_0 \omega \text{Im}[\varepsilon(\mathbf{r})]|\mathbf{E}(\mathbf{r})|^2 \ , \tag{2}$$

where $\text{Im}\,[\varepsilon(\mathbf{r})]$ is the imaginary part of the dielectric function of SRON. Supposing the constant dielectric function over the SRON film section, the heat generated in a domain of SRON beneath the antenna gap (in the domain 1.2 μm $\times$ 1 μm $\times$ 110 nm) is proportional to the square of electric field intensity ($|\mathbf{E}|^2$) integrated over this volume. Consequently,

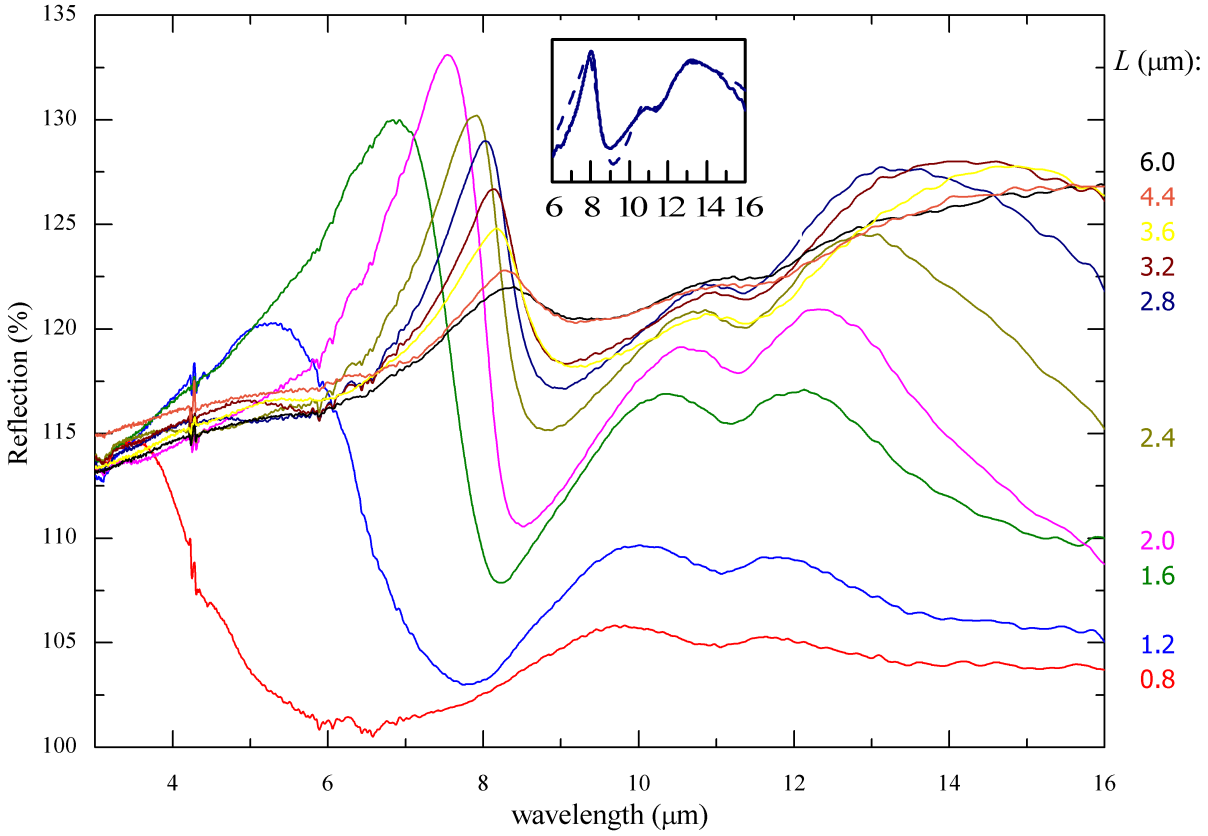

Figure 3: Measured IR unpolarized reflection spectra of dimmer Au antenna arrays of specified arm lengths with the gap 100 nm fabricated on a SRON/Si substrate. The coefficient of filling (by metal area) is the same for all antenna arrays. The particular lengths of antenna arms are denoted on the right side.

the calculated spectra of $|\mathbf{E}|^2$ values averaged over the domain are plotted in Fig. 5 for different arm lengths. In this 3D plot the upper and lower resonance branches are clearly visible. In the lower branch the maximal magnitude of the resonant peaks grows up and the maximum is achieved for the antenna arm length of about 2.4 μm and $\lambda = 7.8$ μm, and equals with the maximum value $|\mathbf{E}_{\rm aver}|^2 = 45$ V^{2}m^{-2}. In the upper branch the maximum reaches $|\mathbf{E}_{\rm aver}|^2 = 38$ V^{2}m^{-2} and appears for $L = 3.6$ μm and $\lambda = 17$ μm.

It is obvious that the positions of maxima are achieved as a result of a trade-off between the size of the antenna (increasing average electric intensity in the gap with the arm length for small antennas) and the material absorption in SRON (decreasing intensity). The slightly smaller maximum intensity in the upper branch compared to the lower one is caused by a higher absorption of IR radiation in SRON at $\lambda = 17.3$ μm with respect to that one at $\lambda = 3.8$ μm.

In addition to the frequency, the heat generation depends on the product of the square of electric field intensity and the imaginary part of the dielectric function of SRON. Therefore, the highest spatially localized enhancement of the absorption in the SRON domain caused by plasmonic resonant effects will occur for the wavelengths already providing an increased absorption of IR radiation in SRON and still reasonable plasmonic resonances in the antennas. Hence, the maximal enhancement of the absorption in the

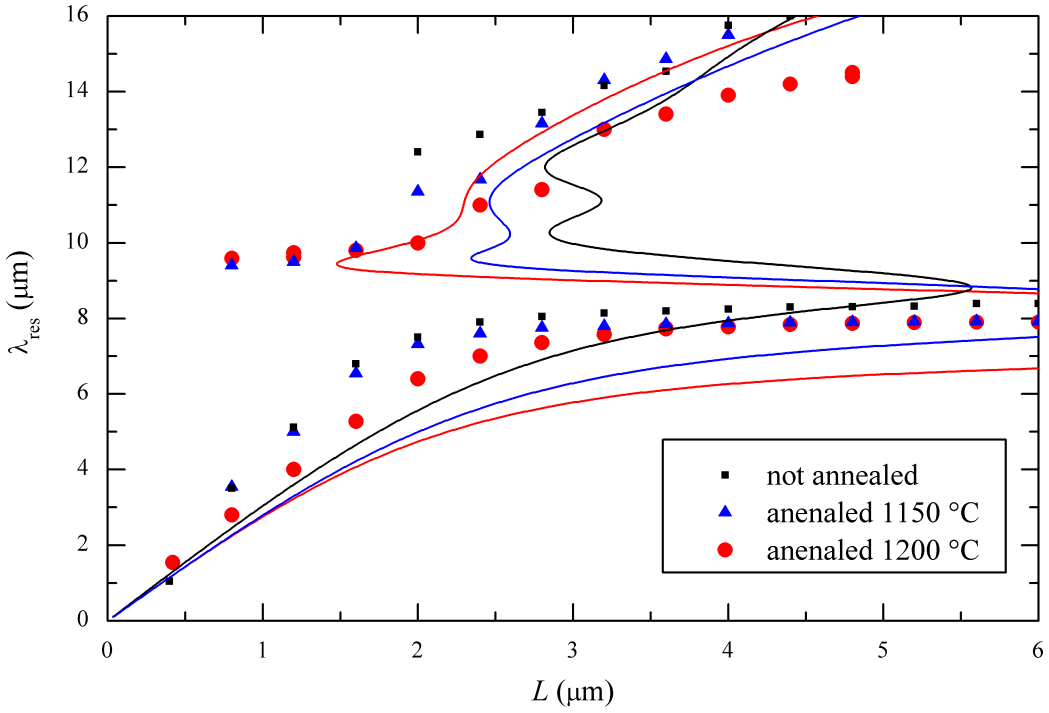

Figure 4: Resonance wavelengths vs. antenna arm lengths L. Experimental data (related to Fig. 3 and 9) and approximative relations (by Equation 1) depicted by dots and curves, respectively.

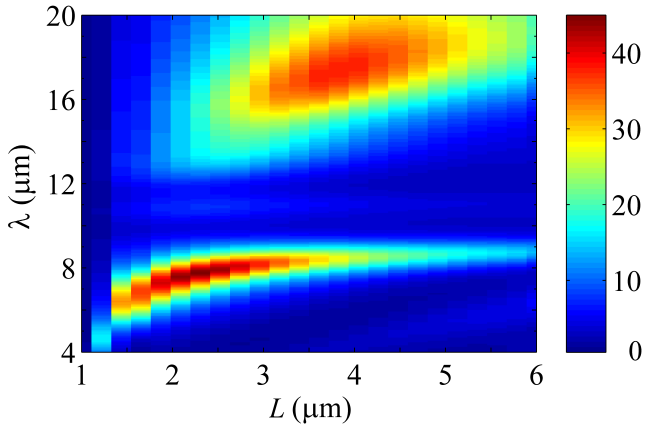

Figure 5: The simulated spectra of the square of the electric field ($|\mathbf{E}|^2$) averaged over a domain (with dimensions 1.2 μm $\times$ 1 μm $\times$ 110 nm) in SRON beneath the antenna gap for different antenna arm lengths specified in Fig. 3 and 4.

SRON domain caused by plasmonic resonant effects is expected in the wavelength intervals 7.8 μm $< \lambda <$ 8.5 μm and $\lambda >$ 12.5 μm where an increased absorption of IR radiation in SRON occurs together with the reasonable resonant peaks of the electric field intensity in the gap.

To find the maximal influence of antennas on enhancement of the absorption in SRON,

the spectra of the relative power absorbed in the SRON domain beneath the antenna gap with respect to that one absorbed in the identical domain without the antenna (on top) was evaluated for antennas of different arm lengths (see Fig. 6 - left). For the lower branch of resonances, the maximum of this relative value reached almost 60 and was achieved for the antenna of the arm length $L = 2.4$ μm and corresponding wavelength $\lambda = 7.8$ μm. For the upper branch this value was 68 and was obtained for the antenna with the arm length $L = 4$ μm and $\lambda = 17.7$ μm.

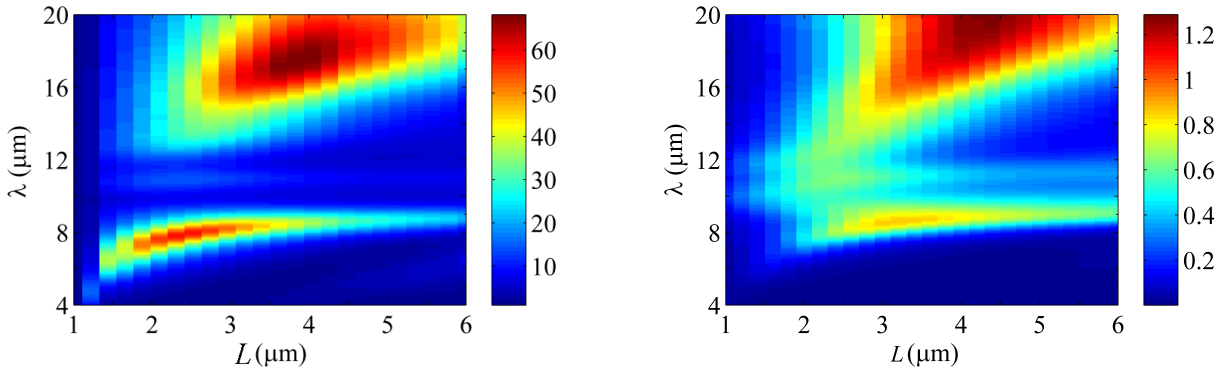

Figure 6: Left: Spectra of the relative power absorbed in the SRON domain beneath the antenna gap with respect to that one absorbed in the identical domain of the sample without the antenna. Right: Absorption efficiency of the SRON domain beneath the antenna gap for different arm lengths of antennas. Measured reflection spectra of simulated antennas are in Fig. 3 (4).

Simultaneously, the absorption efficiency defined as the ratio of the power absorbed in the SRON domain to the energy flux of IR radiation incident on the domain area was evaluated for the antennas of different lengths (see Fig. 6 - right). In the lower branch of resonances, the maximal absorption efficiency reaches a value of 0.86 and occurs for the antenna arm length of 3.2 μm ($\lambda = 8.6$ μm). The maximal absorption calculated in the same SRON domain of the sample without the antenna (bare substrate) was 0.068 and occurred for $\lambda = 9.9$ μm. Hence, the absorption efficiency was enhanced by the plasmonic antennas almost by the factor of 12.6. In the upper branch of resonances, the absorption efficiency of the domain beneath the gap reached the value 1.28 for the antenna arm length of 4.4 μm (about $\lambda = 20$ μm) which represents the enhancement by the factor 19 with respect to the bare SRON.

The relation between the absorption efficiency (Fig. 6 - right) and the square of electric field intensity (see Fig. 5) averaged over a domain beneath the antenna gap in SRON layer is depicted in Fig. 7. The horizontal axis represent the wavelengths of maximal absorption efficiency or maximal averaged electric field intensity for different antenna arm lengths. The figure shows the interplay between the pronounced dispersion of the SRON dielectric function and the electromagnetic resonances of the metallic antenna arms resulting in the red shift between wavelengths for the absorption efficiency related to the maximal averaged electric field intensity.

Finally, to get an overall idea about heat generation by plasmonic processes in the antenna set-up, the FDTD numerical simulations of the heat formed in the metallic antenna arms has been carried out as well. It was found that the heat power developed in the

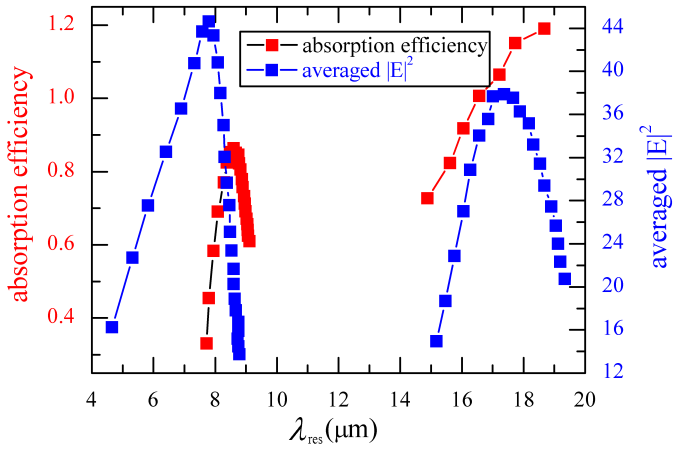

Figure 7: Calculated absorption efficiency and averaged electric field intensity ($|\mathbf{E}^2|$) at resonance wavelengths of different antenna arm lengths.

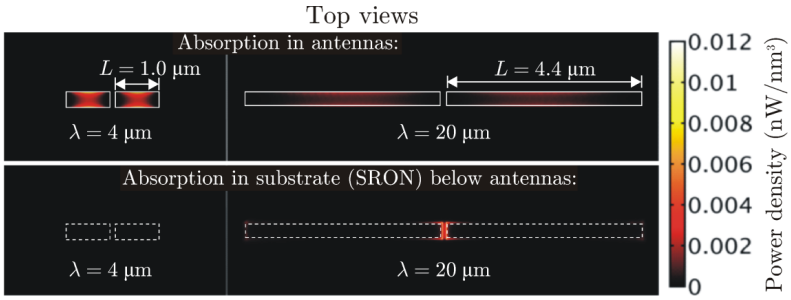

Figure 8: Computed heat power density distribution [nW/nm^3] across the horizontal cross sections in the middle of height of the arms (upper picture) and in the SRON layer 5 nm below the surface (lower picture). The antennas of the length $L = 1$ μm (left) and $L = 4.4$ μm (right) were illuminated by the radiation with the intensity 480 W/cm^2 and wavelengths $\lambda = 4$ μm and $\lambda = 20$ μm, respectively.

antenna arm increases with its length until it reaches its maximum for $L = 2.4$ μm ($\lambda = 7.43$ μm). After that, it starts to decrease steeply. On the other hand, the absorption efficiency (defined as the ratio of the heat power developed in the antenna arm to the energy flux of IR radiation incident on the arm) continuously decreases (from a maximum value of 1.4 for $L = 1$ μm) with the antenna arm length.

Consequently, taking into account the results presented above, there is a chance that at longer wavelengths corresponding to the maximum absorption in SRON beneath the antenna gap the heat developed in this part might be significantly higher than in the antenna arms. Hence, the heating of SRON by the arms would be less significant when the heat in SRON just beneath the antenna gap becomes maximal. The results in Fig. 8 indicate such a spatially localized heat development. In particular, the heat power density distribution (horizontally) across the arms $L = 1$ μm and $L = 4.4$ μm and over SRON beneath the antenna gap is depicted for wavelengths $\lambda = 4$ μm and $\lambda = 20$ μm, respectively.

The discussions on the behaviour of plasmonic resonances of antennas fabricated on the

absorbing substrate and their utilization for spatially localized absorption enhancement of electromagnetic radiation (especially heat generation) in this substrate have been carried out for the mid-IR. However, the conclusions are also applicable for other spectral regions where the materials exhibit a strong absorption resonances (for instance in the visible). The absorption enhancement and efficiency in this region should be even more profound due to correspondingly higher frequencies.

In the following section, the attention will be paid to the interplay between the antenna resonances and the material absorption of various oscillator strengths.

5 IR antennas on an annealed substrate

In the previous Section 4, it was shown that an antenna resonance wavelength is modified remarkably when it approaches a region of the absorption of a surrounding material. The resonance properties of antennas on the absorbing substrate (SRON) discussed in Section 4 are studied in more detail here. Namely, the resonance properties of antennas deposited on SRON annealed at different temperatures (and thus having different absorption peak strengths) are investigated. This investigation of the interplay between plasmonic resonances and (adjustable) resonances in surrounding material can provide supplementary information for sensing application [79], [90].

First, the material changes of SRON during annealing itself are discussed in Section 5.1, and subsequently the resonance properties of antennas deposited on annealed SRON layers are presented in Section 5.2.

5.1 Annealed SRON

SRON can be considered as a multi-phase material composed of a mixture of stoichiometric silicon dioxide (SiO_2), off-stoichiometric oxide (SiO_x, with $x < 2$), elemental silicon, nitrogen and hydrogen [91], [92]. Consequently, SRON shows a pronounced dispersion of its refractive index (and absorption peaks) in infrared [4]. Mutual ratios of bond contents in SRON and the corresponding Lorentz oscillator strengths are tunable by annealing temperatures [91], [92], [93]. Off-stoichiometric oxide and silicon excess are separated into Si nanoclusters (crystalline or amorphous depending on their size), defects (oxidation states) and SiO_2 after the thermal treatment above temperatures of 1000 °C [94], [95], [96].

From the point of view of material changes, this Section 5 is focused on plasmonic sensing of material transformation/modification in SRON occurred by annealing [5]. Furthermore, SRON represents a good material for investigation of the plasmonic enhancement of vibrational modes of surrounding material called Surface-Enhanced Infrared Spectroscopy (SEIRS) studied in following Sections 5.2 and 5.3.

The specimens identical to the ones studied in Section 4 were annealed at temperatures of 1150 °C and 1200 °C. Their dielectric functions were obtained by J. Humlíček via fitting

[4] The structures in the dielectric function of SRON can be tuned by preparation procedures [92].

[5] The results are discussed with respect to photoluminescence measurements performed on bare specimens (without the antennas).

Table 2: Parameters of Lorentz oscillators of fitted reflection of SRON annealed at 1150 °C, where the wavenumber reads $\nu = 1/\lambda$.

$G_m\Omega_m^2$ [10^5cm^{-2}]	ω_{0m} [cm^{-1}]	$\lambda_{0m}(\mu$m)	γ_m [cm^{-1}]
4.70	1066	9.4	88
8.62	939	10.6	222
4.06	442	22.6	131

the reflection by 3 Lorentz oscillators with $\varepsilon_0 = 2.1$ [6]. In particular, the oscillators of specimens annealed at temperatures of 1150 °C and 1200 °C are described by parameters in Tables 2 and 3, respectively.

The oscillators in Tables 1, 2 and 3 can be associated with particular bonds in SRON although it is difficult for its amorphous nature. The first oscillator (at 1066 cm^{-1} and 1078 cm^{-1} for $T_{\text{anneal}} = 1150$ °C and $T_{\text{anneal}} = 1200$ °C) is associated with the stretching mode of Si-O bond. Its frequency moves towards higher energies by annealing and approaches the frequency of 1074 cm^{-1} of a bulk SiO_2 [87]. The second oscillator (at 939 cm^{-1} and 919 cm^{-1} for $T_{\text{anneal}} = 1150$ °C and $T_{\text{anneal}} = 1200$ °C) is associated with Si-O bond [97]. The third oscillator (at 442 cm^{-1} and 452 cm^{-1} for $T_{\text{anneal}} = 1150$ °C and $T_{\text{anneal}} = 1200$ °C) is associated with rocking mode of Si-O bond [98].

The material (and its material phase) changes with annealing that can be observed by a disappearance of the second and third oscillator present in not-annealed SRON. The second oscillator (at 857 cm^{-1}) associated with the stretching mode of Si-N bond [98] disappears as SRON changes from Si_3N_4-like to SiO_2 nature by annealing. Similarly, its third oscillator (at 698 cm^{-1}) associated with neutral oxygen vacancies [87] disappears because its content reduces during annealing resulting in a greater signal from Si-nanoclusters in photoluminescence.

The dielectric functions of not-annealed and annealed SRON are plotted together in Fig. 1. Within the wavelength range of about 8–12.5 μm dielectric functions possess dispersion that is more remarkable for higher annealing temperatures. In particular, SRON has the Reststrahlen band (with possible excitation of surface phonon polaritons) as it obtains properties of SiO_2 by annealing. The quality factors of the first Lorentz oscillators for annealed SRON are two times higher than that one of not-annealed SRON. Moreover, the oscillator strength for the substrate annealed at 1200 °C is two times higher than for the others (compare Tab. 1, 2 with Tab. 3). Moreover, the dispersion in the wavelength range of about 20–26 μm increases from not-annealed to annealed substrate.

The vibration signal in infrared can be enhanced via plasmonic antenna resonance that represents the aim of the next part of this Section 5.2.

5.2 Antenna resonances

The motivation behind is to compare responses of the plasmonic antenna to materials (in its vicinity) having different strengths of absorption peaks. This knowledge can be demanded in sensing applications like SEIRS [67], etc.

This work lies in a comparison of resonances of antennas deposited on SRON layers annealed at different temperatures and thus having different absorption strengths. To per-

[6] The results were confirmed by measurements of the ellipsometry performed by A. Dubroka.

Table 3: Parameters of Lorentz oscillators of fitted reflection of SRON annealed at 1200 °C, where the wavenumber reads $\nu = 1/\lambda$.

$G_m\Omega_m^2$ [10^5cm^{-2}]	ω_{0m} [cm^{-1}]	$\lambda_{0m}(\mu$m)	γ_m [cm^{-1}]
11.1	1078	9.3	71
9.04	919	10.9	252
4.88	452	22.1	88

form this properly, identical arrays of Au antennas have been fabricated by EBL on these specimens. It is worth mentioning fabricated antennas on different specimens should possess almost same dimensions (and geometry). This was managed by a spacer-layer coated on annealed samples below the resist compensating its different adhesion on annealed samples.

Unpolarized reflection spectra were measured by FTIR method on antenna arrays consisted of the same number of antennas [7]. The particular spectra taken from samples not-annealed and annealed at temperatures of 1150 °C and 1200 °C are shown in Fig. 9 a), b) and c), respectively.

The stronger dispersion of dielectric functions (see Fig. 1) of annealed layers results in a deeper dip in reflection spectra (compare Fig. 9 a) with b) and c)) for wavelengths between 7.8–12.5 μm as SRON obtains optical properties similar to SiO_2. The most remarkable dip is observed for the substrate annealed at 1200 °C that may be related to the overdamping of the system [79] associated with higher quality factor and strength of the first Lorentz oscillator of SRON (see Tab. 3). Also, spectra of specimens annealed at 1200 °C possess peaks remarkably sharp and close to ω_{LO} of SiO_2. This behaviour is in agreement with results measured in transmission in [67].

Moreover, one can pay attention to features within the wavelength range of 7.8 μm $< \lambda <$ 9.9 μm corresponding to the Reststrahlen band of annealed SRON (see Fig. 9 b), c)). These features are enhanced only weakly by short antennas possessing plasmonic resonances far below this region. In contrast, they are remarkably enhanced by longer antennas with resonances in this region.

Summarizing, a peak in the region of 7.8 μm $< \lambda <$ 9.9 μm and a dip at $\lambda \sim 12.5$ μm becomes more remarkable on annealed specimens. Therefore, it results in a step in the dependence between resonance wavelengths and antenna arm lengths for annealed SRON in Fig. 4.

Relations between resonance wavelengths and antenna arm lengths are plotted for not-annealed and annealed substrates in Fig. 4. Resonances on annealed layers are blue-shifted in lower and upper branches of resonances. This behaviour was confirmed also by FDTD simulations. In particular, the lower branch of resonances is blue-shifted by presence of stretching mode of Si-O-Si bond. On the other hand, the blue-shift of the upper branch of resonances is determined by the rocking mode of Si-O bond (at about 450 cm^{-1}).

[7] Analogously to Section 4, the reflection spectra acquired from areas with antennas were normalized to reference (bare) spectra without antennas.

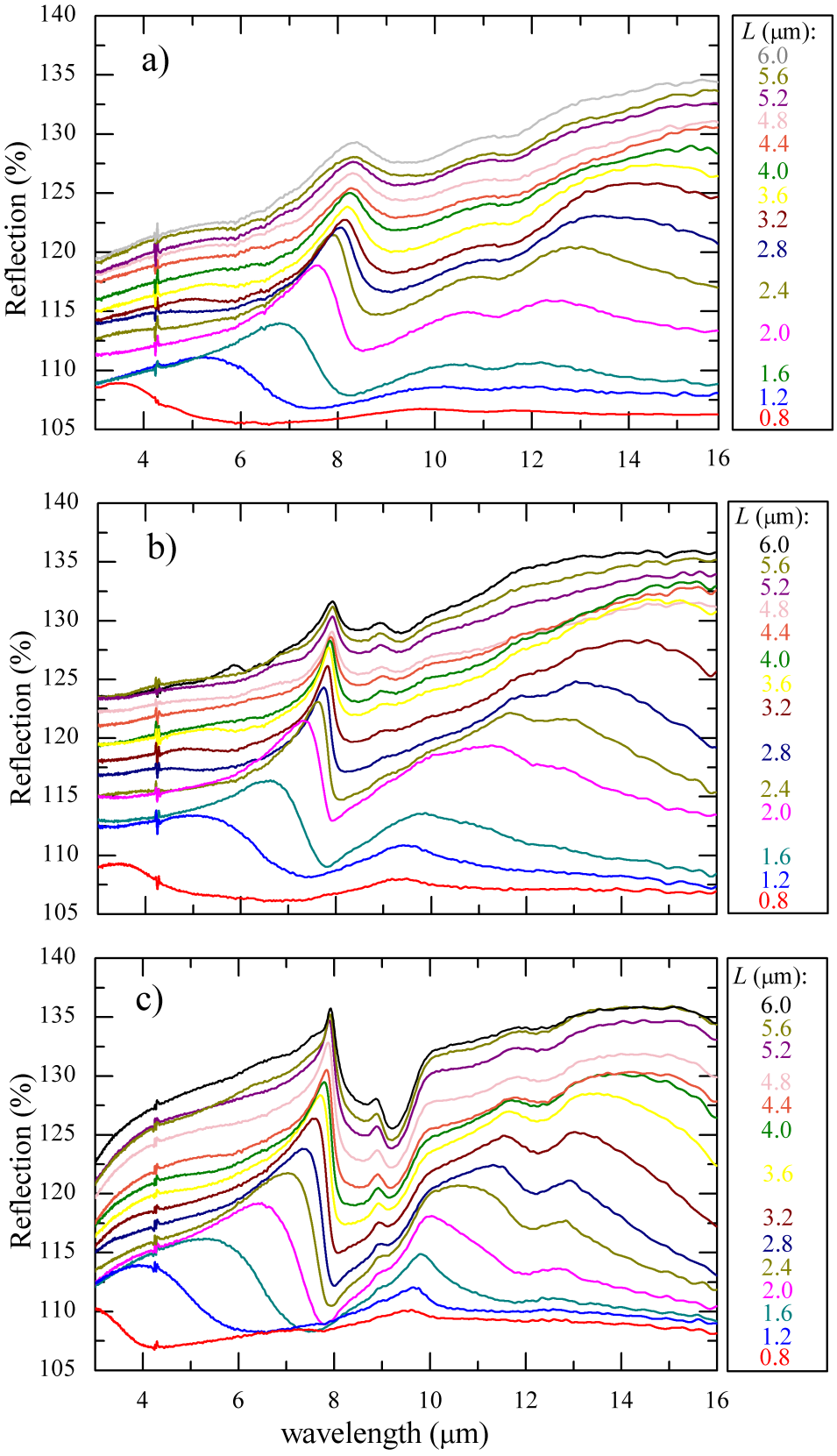

Figure 9: Measured IR unpolarized reflection spectra of dimmer Au antenna (of the gap size of 100 nm) arrays fabricated on a) not-annealed sample, and annealed samples at temperatures b) of 1150 °C and c) of 1200 °C. The particular lengths of antenna arms are denoted on the right side.

5.3 Surface-enhanced infrared spectroscopy on SRON

The plasmonic resonance of an antenna is capable to enhance the vibrational modes of a material in its vicinity. As mentioned above, it is exploited in the Surface-Enhanced Infrared Spectroscopy (SEIRS). Materials with optical properties fitted only by single oscillator were studied by SEIRS in [65], [66], [67]. The "plasmonic" enhancement of a vibrational signal has been represented by the ratio of the height to Full Width at Half Maximum (FWHM) of given spectral features [67].

The SEIRS behaviour can be found also in reflection spectra of antennas on SRON layers (Fig. 9). However, its investigation is more difficult because SRON dielectric function is fitted by 3 or 4 (overlapping) Lorentz oscillators. To approach SEIRS investigation of this material, spectral features enhanced in different wavelength ranges are dealt with independently.

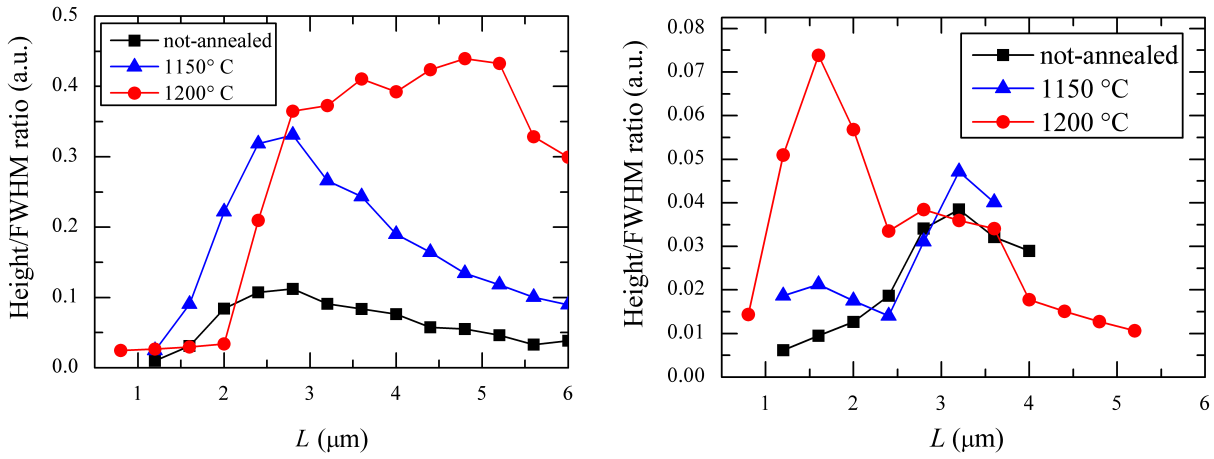

Figure 10: The height-to-FWHM ratios of the features in the lower (left) and upper (right) branches of resonances for different arm lengths. The dependences are plotted for not annealed and annealed SRON layers at temperatures of 1150 °C and 1200 °C.

For the lower branch of resonances, the hight-to-FWHM ratios of peaks in reflection of antennas deposited on not-annealed and annealed SRON are shown in Fig. 10 (left). One should pay attention to not-annealed SRON studied in Section 4. There, the maximal hight-to-FWHM ratio occurs for the antenna arm length of $L = 2.8$ μm that lies between arm lengths of $L = 2.4$ μm and of $L = 3.2$ μm providing maximal electromagnetic field enhancement in metallic arms (proportional to the electric field in SRON domain denoted in Fig. 5) and the absorption efficiency (see Fig. 6) in the SRON layer, respectively. Therefore, the plasmonic antenna resonance is determined by a dielectric function of the surrounding material in its close vicinity where the near field ($\mathbf{E}^2$) is enhanced.

In the upper branch of resonances, the investigation of SEIRS is more difficult because the material resonances of SRON overlap noticeably. The height-to-FWHM ratios of the features are shown for different antenna arm lengths in Fig. 10 (right). There are two peaks for annealed specimens and only one peak for not-annealed SRON. The vibrational peaks enhanced via antennas of about $L = 3.2$ μm correspond to resonance wavelengths of 14.1 μm, 14.3 μm and 12.9 μm for not-annealed and annealed SRON at temperatures of 1150 °C and 1200 °C, respectively. Moreover, spectra of annealed SRON possess peaks

enhanced by antennas of $L = 1.6$ μm corresponding to wavelengths of about 9.7 μm. Before concluding, one should mention a dip in spectra of SRON annealed at 1200 °C. This dip is remarkably enhanced by antennas of $L = 2.8$ μm with correspondent wavelengths of $\sim \lambda = 12.3$ μm [8].

As antennas on SRON annealed at 1200 °C exhibit the most substantial features one can compare their SEIRS spectra for the upper branch of resonances (Fig. 10). Features at wavelengths of about 9.7 μm are enhanced properly by antennas of $L = 1.6$ μm. Going to longer wavelengths, the dip at wavelengths of about $\lambda = 12.3$ μm is properly enhanced by antennas $L = 2.8$ μm while the broad peak is enhanced (only slightly) by the antenna of $L = 3.2$ μm. Summarizing, despite SRON possesses more vibrational modes/peaks, it is possible to find an antenna arm length that enhances the vibrational signal of a given mode properly. More skilful techniques as fitting the reflection spectra or dealing with quality factors of material resonances (its Lorentz oscillators) have not provided deeper insight yet.

6 Conclusions

The presented work deals with the infrared and visible plasmonic antennas for absorption- (Section 4) and sensing-related applications (Section 5). It involves both experimental and theoretical study of plasmonic antennas; the antennas were fabricated, their optical properties were measured and modelled by electromagnetic field simulations [99].

Plasmonic infrared antennas deposited on the SRON layer with a significant absorption in the mid-infrared were studied both for their resonant and absorption properties in Section 4. Almost each reflection spectrum of specific antenna arm length possesses two resonant plasmonic peaks being separated by a dip resulting from a strong coupling of plasmonic oscillations with material absorption resonances in SRON. Consequently, this coupling results in a non-linear scaling between the resonance wavelength and the antenna arm length. Subsequently, the relation between the electric field intensity enhanced by the antenna resonance and the absorption in the SRON layer below antenna were found for different antenna arm lengths. The increased absorption in SRON below the antenna requires both substantial plasmonic resonances and high material absorption of SRON at the same wavelength. The absorption efficiency related to a reference SRON layer reaches its maximal values of 13 at $\lambda = 8.6$ μm ($L = 3.2$ μm), and of 19 at $\lambda = 20$ μm ($L = 4.4$ μm) for lower and upper branches, respectively.

In Section 5, the ability of a plasmonic antenna to enhance a given vibrational mode of its substrate (called SEIRS) was studied and confirmed for SRON annealed at different temperatures (possessing 3-4 material resonances of different strengths). It was shown, that the coupling between the plasmonic resonance and the material oscillations results in not only splitting of the plasmonic resonance (due to the increased absorption of the surrounding material) but also a remarkable excitation of surface phonon polaritons. Moreover, it was found (in Section 5.3) that despite the material possesses more material resonances (described by overlapping Lorentz oscillators), it is possible to find the antenna arm length enhancing the vibrational mode of a given material resonance.

[8] The dip about wavelengths of $\sim \lambda = 12.3$ μm is also weakly observed on SRON annealed at 1150 °C.

So far, the work was focused mainly on resonances of plasmonic antennas on the substrate (SRON) possessing vibrational modes (material resonances) and thus having pronounced dispersion of its refractive index. It has been shown, that the antenna resonance is able to enhance both the absorption in the substrate (with possible temperature increase) and vibrational modes (demanded in sensing applications) in the near- and far-field, respectively. Furthermore, it has been found that despite the presence of more material resonances (described by overlapping Lorentz oscillators), it is still possible to find the antenna arm length enhancing the vibrational mode of a given material resonance. This behaviour is promising in sensing-related applications such as SEIRS. It represents a potential challenge for further study because there are publications aimed at materials with the only one material resonance.

Acknowledgement Práce vznikla za podpory projektu CEITEC (CZ.1.05/1.1.00/02.006) a projektu AMISPEC (TAČR TE01020233).

References

[1] Zenneck J.: Über die fortpflanzung ebener elektromagnetischer wellen längs einer ebenen leiterfläche und ihre beziehung zur drahtlosen telegraphie, *Ann. d. Phys.* **23**, p. 846-866, 1907.

[2] Sommerfeld A.: Jahrbuch d. drahtl. Telegraphie, *Ann. Physik* **28**, p. 665, 1909.

[3] Economou E. N.: Surface Plasmons in Thin Films. *Physical Review* **182** (2), p. 539-554, 1969. DOI: 10.1103/PhysRev.182.539.

[4] Zayats A. V., Smolyaninov I. I., Maradudin A. A.: Nano-optics of surface plasmon polaritons. *Physics Reports* **408** (3-4), p. 131–314, 2005.

[5] Raether H.: Surface Plasmons on Smooth and Rough Surfaces and on Gratings. *Springer Tracts in Modern Physics* **111**, p. 1-133. Springer-Verlag, New York 1988. ISBN 0-387-17363-3.

[6] Berini P.: Plasmon–polariton modes guided by a metal film of finite width. *Optics Letters* **24** (15), p. 1011-1013, 1999. DOI: 10.1364/OL.24.001011.

[7] Maier S. A.: *Plasmonics: Fundamental and Applications.* Springer, Bath-UK, 2007. ISBN-10: 0387331506.

[8] Wood R. W.: On a remarkable case of uneven distribution of light in a diffraction grating spectrum. *Phil. Mag.* **4**, p. 396-402, 1902.

[9] Powell C. J., Swan J. B.: Origin of the Characteristic Electron Energy Losses in Aluminum. *Phys. Rev.* **115**, p. 869-875, 1959.

[10] Ritchie, R. H.: Plasma losses by fast electrons in thin films. *Physical Review* **106** (5), p. 874–881, 1957. DOI: 10.1103/PhysRev.106.874.

[11] Kretschmann E., Reather H.: Radiative decay of non radiative plasmons excited by light. *Zeitschrift für Naturforschung* **23A**, p. 2135-2136, 1968.

[12] Otto A.: Excitation of nonradiative surface plasma waves in silver by the method of frustrated total reflection. *Zeitschrift für Physik* **216**, p. 398-410, 1968.

[13] Zia R., Schuller J. A., Chandran A., Brongersma M. L.: Plasmonics: the next chip-scale technology. *Materials Today* **9** (7-8), 2006. DOI: 10.1016/S1369-7021(06)71572-3

[14] Stockman M. I.: Nanoplasmonics: The physics behind the applications. *Physics Today* **64** (2), p. 39-44, 2011. doi.org/10.1063/1.3554315

[15] Krenn J.: Perspective on plasmonics. *Nature Photonics* **6**, p. 714–715, 2012. doi:10.1038/nphoton.2012.275

[16] Dionne J. A., Diest K., Sweatlock L. A., Atwater H. A.: PlasMOStor: A Metal-Oxide-Si Field Effect Plasmonic Modulator. *Nano Letters* **9** (2), p. 897–902, 2009.

[17] Stockman M. I.: An easier route to high harmony. *Nature* **453**, 2008.

[18] Neutens P., Van Dorpe P., De Vlaminck I., Lagae L., Borghs G.: Electrical detection of connected gap plasmons in metal–insulator–metal waveguides. *Nature Photonics* **3**, p.283, 2009.

[19] Dionne J. A., Diest K., Sweatlock L. A., Atwater H. A.: *NanoLetters* **9**, p. 897, 2009.

[20] Dvořák P., Neuman T., Břínek L., Šamořil T., Kalousek R., Dub P., Varga P., Šikola T.: Control and Near-Field Detection of Surface Plasmon Interference Patterns. NanoLetters **13**, 2558-2563, 2013.

[21] Lal S., Link S., Halas N. J.: Nano-optics from sensing to waveguiding. *Nature Nanophotonics* **1**, p. 641-648, 2007. doi:10.1038/nphoton.2007.223

[22] Homola J., Yeea S. S., Gauglitzb G.: Surface plasmon resonance sensors: review. *Sensors and Actuators B: Chemical* **54** (1-2), p. 3-15, 1999.

[23] Lal S., Clare S. E., Halas N. J.: Nanoshell-Enabled Photothermal Cancer Therapy: Impending Clinical Impact. *Acc. Chem. Res.* **41** 12, p. 1842-1851, 2008.

[24] Bharadwaj P., Deutsch B., Novotny L.: Optical antennas. *Advances in Optics and Photonics* **1**, p. 438–483, 2009. DOI:10.1364/AOP.1.000438.

[25] Biagioni P., Huang J.-S., Hecht B.: Nanoantennas for visible and infrared radiation. *Report Progress Physics* **75** (2), 024402, 2012. DOI: 10.1088/0034-4885/75/2/024402.

[26] Novotny L., van Hulst N.: Antennas for light. *Nature Photonics* **5** (2), p. 83-90, 2011. DOI: 10.1038/NPHOTON.2010.237.

[27] Novotny L.: From near-field optics to optical antennas. *Physics Today* **64** (7), p. 47-52, 2011.

[28] Berkovitch N., Ginzburg P., Orenstein M.: Nano-plasmonic antennas in the near infrared regime. *Journal of Physics: Condensed Matter* **24** (7), 073202, 2012.

[29] Mayer K. M., Hafner J. H.: Localized Surface Plasmon Resonance Sensors. *Chemical Reviews ACS* **111**, p. 3828–3857, 2011.

[30] Taubner T., Keilmann F., Hillenbrand R.: Nanoscale-resolved subsurface imaging by scattering-type near-field optical microscopy. *Optics Express* **13** (22), 2005.

[31] Grober R. D., Schoelkopf R. J., Prober D. E.: Optical antenna: Towards a unity efficiency near-field optical probe. *Applied Physics Letters* **70** (11), p. 1354-1356, 1997. DOI: 10.1063/1.118577.

[32] Stockle R. M., Suh Y. D., Deckert V., Zenobi R.: Nanoscale chemical analysis by tip-enhanced Raman spectroscop. *Chemical Physics Letters* **318**, p. 131–136, 2000.

[33] Atwater H. A., Polman A.: Plasmonics for improved photovoltaic devices. *Nature Materials* **9**, p. 205-213, 2010. doi: 10.1038/nmat2629

[34] Ferry V. E., Munday J. N., Atwater H. A.: Design Considerations for Plasmonic Photovoltaics. *Advanced Materials* **22**, p. 4794-4808, 2010. DOI: 10.1002/adma.201000488

[35] Pillai S., Catchpole K. R., Trupke T., Green M. A.: Surface plasmon enhanced silicon solar cells. *Journal of Applied Physics* **101**, 093105, 2007.

[36] Biteen J. S., Sweatlock L. A., Mertens H., Lewis N. S., Polman A., Atwater H. A.: Plasmon-Enhanced Photoluminescence of Silicon Quantum Dots: Simulation and Experiment. *Journal of Physical Chemistry C* **111** (36), 13372-13377, 2007.

[37] Mertens H., Koenderink A. F., Polman A.: Plasmon-enhanced luminescence near noble-metal nanospheres: Comparison of exact theory and an improved Gersten and Nitzan model. *Physical Review B* **76**, 115123, 2007.

[38] Novotny, L., Bian, R. X., Xie, X. S.: Theory of nanometric optical tweezers. *Phys. Rev. Lett.* **79**, p. 645–648, 1997.

[39] Righini, M., Zelenina, A. S., Girard, C., Quidant R.: Parallel and selective trapping in a patterned plasmonic landscape. *Nature Phys.* **3**, p. 477–480, 2007.

[40] Righini, M., Volpe, G., Girard, C., Petrov, D., Quidant, R.: Surface plasmon optical tweezers: tunable optical manipulation in the femtonewton range. *Physical Review Letters* **100**, 183604, 2008.

[41] Baffou G., Quidant R., Girard C.: Heat generation in plasmonic nanostructures: Influence of morphology. *Applied Physics Letters* **94** (15), 153109, 2009. DOI: 10.1063/1.3116645.

[42] Baffou G., Quidant R., Girard Ch.: Thermoplasmonics modeling: A Green's function approach. *Physical Review B* **82** (16), 165424, 2010. DOI: 10.1103/PhysRevB.82.165424.

[43] Baffou G., Kreuzer M. P., Kulzer F., Quidant R.: Temperature mapping near plasmonic nanostructures using fluorescence polarization anisotropy. *Optics Express* **17** (5), 2009.

[44] Huang X., Qian W., El-Sayed I. H., El-Sayed M. A.: The potencial use of the enhanced nonlinear properties of gold nanosphere in photothermal cancer therapy. *Lasers Surg. Med.* **39** (9), 747-753, 2007.

[45] Muhlschlegel P., Eisler H.-J., Martin O. J. F., Hecht B.: Resonant Optical Antennas. *Science* **308**, 2005.

[46] Sládková L., Képeš E.; Břínek L., Prochazka D., Novotný J., Kaiser J.: Detekcia stopových prvkov metódou spektroskopie laserom indukovanej mikroplazmy (LIBS) pomocou aplikácie nanočastíc. *Jemná mechanika a optika*, **59** (6-7), p. 201-203, 2014. ISSN: 0447- 6441.

[47] Gonzalez F. J., Boreman G.D.: Comparison of dipole, bowtie, spiral and log-periodic IR antennas. *Infrared Physics Technology* **46** (5), p. 418-428, 2005. DOI: 10.1016/j.infrared.2004.09.002.

[48] Govorov A. O., Richardson H. H.: Generating heat with metal nanoparticles. *Nanotoday* **2** (1), p. 30-38, 2007. DOI: 10.1016/S1748-0132(07)70017-8.

[49] Baffou G., Girard Ch., Quidant R.: Mapping Heat Origin in Plasmonic Structures. *Physical Review Letters* **104**, 136805, 2010.

[50] Schmuttenmaer Ch. A.: Exploring Dynamics in the Far-Infrared with Terahertz Spectroscopy. *Chem. Rev.* **104**, 1759-1779, 2004.

[51] Richards P. L.: Bolometers for infrared and millimeter waves. *J. App. Phys.* **76** (1), 1994.

[52] Gonzalez F. J., Ashley C. S., Clem P. G., Boreman G.D.: Antenna-coupled microbolometer arrays with aerogel thermal isolation. *Infrared Physics & Technology* **45**, 47–51, 2004.

[53] Cao L., Barsic D. N., Guichard A. R., Brongersma M. L.: Plasmon-Assisted Local Temperature Control to Pattern Individual Semiconductor Nanowires and Carbon Nanotubes. *NanoLetters* **7** (11), 3523-3527, 2007.

[54] Richardson H. H., Hickman Z. N., Govorov A. O., Thomas A. C., Zhang W., Kordesch M. E.: Thermooptical Properties of Gold Nanoparticles Embedded in Ice: Characterization of Heat Generation and Melting. *NanoLetters* **6** (4), 783-788, 2006.

[55] Le F., Brandl D. W., Urzhumov,Y. A., Wang H., Kundu J., Halas N. J., Aizpurua J., Nordlander P.: Metallic Nanoparticle Arrays: A Common Substrate for Both Surface-Enhanced Raman Scattering and Surface-Enhanced Infrared Absorption. *ACS Nano* **2** (4), p. 707–718, 2008.

[56] Kneipp K., Wang Y., Kneipp H., Perelman L. T., Itzkan I., Dasari R. R., Feld M. S.: Single Molecule Detection Using Surface-Enhanced Raman Scattering (SERS). *Physical Review Letters* **78** (9), p. 1667-1670, 1997.

[57] Nie S., Emory S. R.: Probing Single Molecules and Single Nanoparticles by Surface-Enhanced Raman Scattering. *Science* **275**, 1997.

[58] Novotny L., Hecht B.: *Principles of Nano-Optics.* Cambridge University Press. ISBN 9780521539883, 2006.

[59] Li J. F., Huang Y. F., Ding Y., Yang Z. L., Li S. B., Zhou X. S., Fan F. R., Zhang W., Zhou Z. Y., Wu D. Y., Ren B., Wang Z. L., Tian Z. Q.: Shell-isolated nanoparticle-enhanced Raman spectroscopy. *Nature* **464**, p. 392-395, 2010.

[60] Xu H., Aizpurua J., Kall M., Apell P.: Electromagnetic contributions to single-molecule sensitivity in surface-enhanced Raman scattering. *Physical Review E* **62** (3), 2000.

[61] Pettinger B., Ren B., Picardi G., Schuster R., Ertl G.: Nanoscale Probing of Adsorbed Species by Tip-Enhanced Raman Spectroscopy. *Physical Review Letters* **92** (9), 2004.

[62] Cancado L. G., Hartschuh A., Novotny L.: Tip-enhanced Raman spectroscopy of carbon nanotubes. *J. Raman Spectrosc.* **40**, p. 1420–1426, 2009.

[63] Adato R., Altug H.: In-situ ultra-sensitive infrared absorption spectroscopy of biomolecule interactions in real time with plasmonic nanoantennas. *Nature Communications* **4**, p. 2154, 2013. DOI: 10.1038/ncomms3154

[64] Hillenbrand R., Taubner T., Keilmann F.: Phonon-enhanced light–matter interaction at the nanometre scale. Nature **418**, p. 159-162, 2002.

[65] Neubrech F., Pucci A., Cornelius T.W., Karim S., García-Etxarri A., Aizpurua J.: Resonant Plasmonic and Vibrational Coupling in a Tailored Nanoantenna for Infrared Detection. *Physical Review Letters* **101**, 157403, 2008.

[66] Neubrech F., Weber D., Enders D., Nagao T., Pucci A.: Antenna Sensing of Surface Phonon Polaritons. *J. Phys. Chem. C*, **114**, p. 7299–7301, 2010.

[67] Neubrech F., Pucci A.: Plasmonic Enhancement of Vibrational Excitations in the Infrared. *IEEE Journal of selected topics in quantum electronics* **19**, 3, 2013.

[68] Gigler A. M., Huber A. J., Bauer M., Ziegler A., Hillenbrand R., Stark R. W.: Nanoscale residual stress-field mapping around nanoindents in SiC by IR s-SNOM and confocal Raman microscopy. *Optics Express* **17** (25), 2009.

[69] Brehm M., Taubner T., Hillenbrand R., Keilmann F.: Infrared Spectroscopic Mapping of Single Nanoparticles and Viruses at Nanoscale Resolution. *NanoLetters* **6** (7), 2006.

[70] Schnell M., García-Etxarri A., Huber A. J., Crozier K., Aizpurua J., Hillenbrand R.: Controlling the near-field oscillations of loaded plasmonic nanoantennas. *Nature Photonics* **3**, p. 287-291, 2009. doi:10.1038/nphoton.2009.46

[71] Huang J.-S., Kern J., Geisler P., Weinmann P., Kamp M., Forchel A., Biagioni P., Hecht B.: Mode Imaging and Selection in Strongly Coupled Nanoantennas. *NanoLetters* **10** (6), p. 2105–2110, 2010.

[72] Prodan E., Radloff C., Halas N. J., Nordlander P.: A Hybridization Model for the Plasmon Response of Complex Nanostructures. *Science* **302** (5644), p. 419-422, 2003.

[73] Bryant G. W., de Abajo F. J. G., Aizpurua J.: Mapping the Plasmon Resonances of Metallic Nanoantennas. *NanoLetters* **8** (2), p. 631–636, 2008.

[74] Ai Leen Koh, Bao K., Khan I., Smith W. E., Kothleitner G., Nordlander P., Maier S. A., and McComb D. W.: Electron Energy-Loss Spectroscopy (EELS) of Surface Plasmons in Single Silver Nanoparticles and Dimers: Influence of Beam Damage and Mapping of Dark Modes. *ACS Nano* **3** (10), p. 3015–3022, 2009.

[75] Spinelli P., van Lare C., Verhagen E., Polman A.: Controlling Fano lineshapes in plasmon-mediated light coupling into a substrate. *Optics Express* **19**, S3, 2011.

[76] Verellen N., Sonnefraud Y., Sobhani H., Hao F., Moshchalkov V. V., Van Dorpe P., Nordlander P., Maier S. A.: Fano Resonances in Individual Coherent Plasmonic Nanocavities. *NanoLetters* **9** (4), p. 1663-1667, 2009.

[77] Crozier K. B., Sundaramurthy A., Kino G. S., and Quate C. F.: Optical antennas: Resonators for local field enhancement. *Journal of Applied Physics* **94** (7), p. 4632-4642, 2003. DOI: 10.1063/1.1602956.

[78] Šikola T., Kekatpure R. D., Barnard E. S., White J. S., Dorpe P. Van, Břínek L., Tomanec O., Zlámal J., Lei D., Sonnefraud Y., Maier S. A., Humlíček J., Brongersma M. L.: Mid - IR plasmonic antennas on silicon-rich oxinitride absorbing substrates: nonlinear scaling of resonance wavelengths with antenna length. *Applied Physics Letters* **95** (25), 253109, 2009. doi:10.1063/1.3278593

[79] Adato R. Artar A., Erramilli A., Altug H.: Engineered absorption enhancement and induced transparency in coupled molecular and plasmonic resonator systems. *NanoLetters* **13**, p. 2584-2591, 2013.

[80] Brown L.V., Zhao Ke, King N., Sobhani H., Nordlander P., Halas N. J.: Surface-Enhanced Infrared Absorption Using Individual Cross Antennas Tailored to Chemical Moieties. *J. Am. Chem. Soc.* **135**, p. 3688-3695, 2013.

[81] Alonso-González P., Albella P., Neubrech F., Huck C., Chen J., Golmar F., Casanova F., Hueso L. E., Pucci A., Aizpurua J., Hillenbrand R.: Experimental Verification of the Spectral Shift between Near- and Far-field Peak Intensities of Plasmonic Infrared Nanoantennas. *Physical Review Letters* **110**, 203902, 2013.

[82] Břínek L., Šamořil T., Tomanec O., Hrton M., Kalousek R., Spousta J., Dub P., Varga P., Šikola T.: Plasmon Resonances of Mid-IR Antennas on an Absorbing Substrate: Optimization of Localized Absorption Enhancement. To be submitted, 2015.

[83] Hägglund C., Kasemo B.: Nanoparticle Plasmonics for 2D-Photovoltaics: Mechanisms, Optimization, and Limits. *Optics Express* **17** (14), p. 11944-11957, 2009.

[84] Codreanu I., Boreman G. D.: Infrared Microstrip Dipole Antennas - FDTD Predictions versus Experiment. *Microwave and Optical Technology Letters* **29** (6), 2001.

[85] Tsu D. V., Lucovsky G., Mantini M. J.: Local atomic structure in thin films of silicon nitride and silicon diimide produced by remote plasma-enhanced chemical-vapor deposition. Physical Review B **33** (10), 1986.

[86] Ribeiro M., Pereyra I., Alayo M.I.: Silicon rich silicon oxynitride films for photoluminescence applications. *Thin Solid Films* **426**, p. 200–204, 2003.

[87] Luna-López J. A., Carrillo-López J., Aceves-Mijares M., Morales-Sánchez A., Falcony C.: FTIR and photoluminescence of annealed silicon rich oxide films. *Superficies y Vacío* **22** (1), p. 11-14, 2009.

[88] Dintinger J., Klein S., Bustos F., Barnes W. L., and Ebbesen T. W.: Strong coupling between surface plasmon-polaritons and organic molecules in subwavelength hole arrays. *Phys. Rev. B* **71**, 035424, 2005.

[89] F. D. T. D. Solutions (version 7.5.5), from Lumerical Solutions, Inc., http://www.lumerical.com.

[90] Azarova N., Ferguson A. J., van de Lagemaat J., Rengnath E., Park W., Johnson J. C.: Coupling between a Molecular Charge-Transfer Exciton and Surface Plasmons in a Nanostructured Metal Grating. *J. Phys. Chem. Lett.* **4**, p. 2658-2663, 2013.

[91] Kohli S. at all.: Nanocrystal formation in annealed a-SiO0.17 N0.07:H films. *Nanotechnology* **15**, p. 1831–1836, 2004.

[92] Habraken F. H. P. M.: Characterization of LPCVD and PECVD silicon oxinitride. *Applied Surface Science* **30**, p. 186-196, 1987.

[93] Wong C. K. at all.: Fabrication of Optical Waveguide using Silicon Oxynitride Prepared by Thermal Oxidation of Silicon Rich Silicon Nitride. *IEEE, 0-7803-9339-2/05*, 2005.

[94] Hussein M. G., Worhoff K., Sengo G., Driessen A.: Optimization of plasma-enhanced chemical vapor deposition silicon oxynitride layers for integrated optics applications. *Thin Solid Films* **515**, p. 3779-3786, 2007.

[95] Kohli S., Theil J. A., Dippo P. C., Jones K. M., Al-Jassim M. M., Ahrenkiel R. K., Rithner Ch. D., Dorhout P. K.: Nanocrystal formation in annealed a-SiO0.17N0.07:H films. *Nanotechnology* **15**, p. 1831–1836, 2004.

[96] Lee J. H., Jeong Ch. H., Lim J. T., Zavaleyev V. A., Min K. S., Kyung S. J., Yeom G. Y.: Characteristics of SiOxNy Films Deposited by PECVD at Low-Temperature Using BTBAS-NH3-O2. *Journal of the Korean Physical Society* **48** (1), 2006.

[97] Zhu M., Han Y., Wehrspohn R. B., Godet C., Etemadi R., Ballutaud D.: The origin of visible photoluminescence from silicon oxide thin films prepared by dual-plasma chemical vapor deposition. *Journal of Applied Physics* **83** (10), 1998.

[98] Tsu D. V., Lucovsky G., Davidson B. N.: Effects of the nearest neighbors and the alloy matrix on SiH stretching vibrations in the amorphous SiOr:H (0¡r¡2) alloy system. *Phys. Rev. B* **40**, p. 1795, 1989.

[99] Kalousek R., Dub P., Břínek L., Šikola T.: Response of plasmonic resonant nanorods: an analytical approach to optical antennas. *Optics Express* **20** (16), p.17916-17927, 2012.

7 Author's Publications

[J1] Tomanec O., Hrnčíř T., Lovicar L., Šustr L., Břínek L., Kalousek R., Chmelík R., Spousta J., Šikola T.: Studium vlastností mikro- a nanostruktur v oblasti plazmoniky na Ústavu fyzikálního inženýrství FSI VUT v Brně. Jemná mechanika a optika, roč. 52, č. 6, s. 187-189, 2008. ISSN: 0447- 6441.

[J2] [78] Šikola T., Kekatpure R. D., Barnard E. S., White J. S., Dorpe P. Van, Břínek L., Tomanec O., Zlámal J., Lei D., Sonnefraud Y., Maier S. A., Humlíček J., Brongersma M. L.: Mid - IR plasmonic antennas on silicon-rich oxinitride absorbing substrates: nonlinear scaling of resonance wavelengths with antenna length. Applied Physics Letters **95** (25), 253109, 2009. doi:10.1063/1.3278593

[J3] Škoda D., Kalousek R., Tomanec O., Bartošík M., Břínek L., Šustr L., Šikola T.: Studium optických vlastností nanostruktur pomocí mikroskopie blízkého pole. Jemná mechanika a optika, roč. 54, č. 7-8, s. 219-222, 2009. ISSN: 0447- 6441.

[J4] [99] Kalousek R., Dub P., Břínek L., Šikola T.: Response of plasmonic resonant nanorods: an analytical approach to optical antennas. Optics Express **20** (16), 17916-17927, 2012.

[J5] Břínek L., Dvořák P., Neuman T., Dub P., Kalousek R., Šikola T.: Aplikace rastrovací optické mikroskopie v blízkém poli pro plasmoniku. Jemná mechanika a optika, roč. 58, č. 6, s. 169-171, 2013, ISSN: 0447- 6441.

[J6] [20] Dvořák P., Neuman T., Břínek L., Šamořil T., Kalousek R., Dub P., Varga P., Šikola T.: Control and Near-Field Detection of Surface Plasmon Interference Patterns. NanoLetters **13**, 2558-2563, 2013.

[J7] Břínek L., Édes, Z., Dvořák P., Neuman T., Šamořil T., Kalousek R., Dub P., Šikola T.: Interference povrchových plazmonů v blízkém poli. Československý časopis pro fyziku, roč. 63, č. 4, s. 234-236, 2013. ISSN: 0009- 0700.

[J8] [46] Sládková L., Képeš E.; Břínek L., Prochazka D., Novotný J., Kaiser J.: Detekcia stopových prvkov metódou spektroskopie laserom indukovanej mikroplazmy (LIBS) pomocou aplikácie nanočastíc. Jemná mechanika a optika, roč. 59, č. 6-7, s. 201-203, 2014. ISSN: 0447- 6441.

[J9] Křápek V., Koh A., Břínek L., Hrtoň M., Tomanec O., Kalousek R., Maier S., Šikola T.: Spatially resolved electron energy loss spectroscopy of crescent- shaped plasmonic antennas. Optics Express **23** (9), 11855-11867, 2015. ISSN: 1094-4087

[J10] [82] Břínek L., Šamořil T., Tomanec O., Hrton M., Kalousek R., Spousta J., Dub P., Varga P., Šikola T.: Plasmon Resonances of Mid-IR Antennas on an Absorbing Substrate: Optimization of Localized Absorption Enhancement. To be submitted, 2015.

8 Project grants

[P1] 2009: Project of FME, BUT: "Studium plazmonických struktur vytvořených fokusovaným iontovým svazkem."

[P2] 2010: European Science Foundation (Ref. N. 3569): "FDTD Simulations of Plasmonic Structures On Membranes."

9 Author's Curriculum Vitae

- 1. 9. 2003 - 10. 6. 2008: Master's degree.
- 1. 03. 2007 - 31. 8. 2007: Erasmus, TU/E, Eindhoven, Netherlands. Giant 'Dry' Actuation of PEDOT:PSS thin films.
- 16. 7. 2008 - 31. 8. 2015: Doctoral degree.
- 4. 07. 2010 - 18. 07. 2010: ESF: Short Visit Grant, 3569. Imperial College London, London, GB. FDTD Simulations of Plasmonic Structures On Membranes.

10 Abstract

Práce pojednává o vlastnostech plazmonických antén v infračervené a viditelné oblasti. Práce zahrnuje výrobu, měření a numerické modelování optických vlastností antén. Infračervené plazmonické antény na absorbujícím substrátu (SRON) jsou studovány pro jejich rezonanční a absorpční vlastnosti. Byla nalezena geometrie antény, která poskytuje maximální účinnost absorpce ve SRON vrstvě. Dále je studována možnost zesílení daného vibračního módu substrátu (obsahujícího 3-4 materiálové rezonance) pomocí plazmonické rezonance antény.

The work deals with plasmonic antennas for infrared and visible wavelengths. This work involves fabrication, measurements and numerical modelling of optical properties of these structures. First, infrared plasmonic antennas deposited on the SRON layer with a significant absorption are studied both for their resonant and absorption properties. The antenna geometry providing maximal enhancement of the absorption efficiency in the SRON layer is found. Subsequently, the ability of a plasmonic antenna resonance to enhance a given vibrational mode of its substrate (called SEIRS) possessing 3-4 material resonances is studied and confirmed on antennas on SRON.